LWT - Food Science and Technology 153 (2022) 112473

Contents lists available at ScienceDirect

LWT

journal homepage: www.elsevier.com/locate/lwt

Viscoelastic behavior and fouling propensity of concentrated suspended particles of orange juice with defined size distributions: Towards a better control of the deposit layer properties during microfiltration

Camille Demoulin [b], Christelle Wisniewski [b], Julien Ricci [a,b], Michèle Delalonde [b], Layal Dahdouh [a,b,*]

[a] CIRAD, UMR Qualisud, F-34398 Montpellier, France
[b] Qualisud, Université de Montpellier, Avignon Université, CIRAD, Institut Agro, IRD, Université de La Réunion, Montpellier, France

A R T I C L E I N F O

Keywords:
Solid-like behavior
Specific resistance to filtration
Deposit layer compressibility
Orange juice microfiltration
Particle size distribution

A B S T R A C T

This work aimed at characterizing the viscoelastic behavior and the fouling propensity of orange juice matrices composed of concentrated suspended particles (CSP) with defined size distributions. Small-, medium- and large-CSP (respectively colloids, supra-colloids and large particles) were first isolated and then mixed together according to a mixture design. The shear moduli, the specific resistance to filtration and the compressibility factor of isolated CSP and CSP mixtures were quantified. Small-, medium- and large-CSP were characterized by viscoelastic properties with a predominant solid-like behavior. The deposit layer of large-CSP had the highest shear moduli, while small-CSP presented the highest specific resistance to filtration. Small-, medium- and large-CSP deposit layers were considered as compressible matrices. The rheological behavior and the fouling propensity of mixtures of small-, medium- and large-CSP were analyzed using ternary diagrams. These diagrams revealed that the small-, medium- and large-CSP proportions modulated differently the shear moduli and the fouling propensity of CSP mixtures. Indeed, the solid-like behavior was strongly influenced by large-CSP proportions, the specific resistance to filtration depended mainly on the CSP size polydispersity, while small- or medium-CSP proportions had a major influence on the compressibility factor.

1. Introduction

Pressure-driven membrane technologies are widely used in the fruit juices processing chain, as they offer various applications, from macroscopic separation (e.g. concentration, clarification, fractionation) to specific isolation and purification operations (e.g. aroma recovery, sugar content regulation, bioactive compounds purification). Ultrafiltration and nanofiltration are used to isolate and/or purify specific compounds, whereas microfiltration is commonly used to concentrate some large bioactive compounds in the pulpy fractions and/or to produce in a single step a microbiological stabilized and clarified juice (de Oliveira et al., 2012; Laorko et al., 2013; Vaillant et al., 2005). During microfiltration, a decrease in the permeate flux is observed over time, leading to a drastic reduction in the productivity due to the well-known membrane fouling phenomenon (Razi et al., 2012).

Fruit-based suspensions, well known to be heterogeneous systems containing colloids, supracolloids and large particles suspended in a continuous aqueous phase, are considered as highly-fouling suspensions (Rouquié et al., 2019). During the microfiltration of such complex suspensions, the deposit formation due to the larger suspended particles accumulation onto the membrane surface is considered as one of the main causes of membrane fouling (Bhattacharjee et al., 2017; Miyoshi et al., 2015). Several approaches and operating strategies are commonly adopted to limit this deposit layer. For example, crossflow filtration is conventionally used to enhance shear rate close to the membrane surface, and consequently increase the back-transport of juice particles from the membrane vicinity (Kazemi et al., 2012). The different mechanisms for back-transport (e.g. Brownian diffusion, shear-induced diffusion or inertial lift (Davis, 1992)) can occur concurrently, thereby reducing retention of particles (i.e. colloids, supracolloids or large particles) on the membrane surface (Kromkamp et al., 2006). In addition to mechanical actions promoting the back-transport of particles away from the membrane, treatments prior to microfiltration (i.e. coarse filtration, centrifugation, flocculation by gelatin and/or bentonite, enzymatic

* Corresponding author. Qualisud, Université de Montpellier, Avignon Université, CIRAD, Institut Agro, IRD, Université de La Réunion, Montpellier, France.
E-mail address: layal.dahdouh@cirad.fr (L. Dahdouh).

https://doi.org/10.1016/j.lwt.2021.112473
Received 26 May 2021; Received in revised form 13 August 2021; Accepted 14 September 2021
Available online 15 September 2021

treatment, ultrasound) can be used to minimize fouling. They can reduce not only the concentration of suspended particles in the feed (de Oliveira et al., 2012; Ushikubo et al., 2007; Vaillant et al., 1999; Yu & Lencki, 2004), but also modify the size distribution of these suspended particles. The modification of the suspended particles size distribution is of great interest, since the efficiency of the back-transport phenomena in keeping particles away from the membrane, and consequently to limit their accumulation on the membrane, is strongly linked to particle size (Davis, 1992).

Since monitoring the suspended particles size distribution of the feed (i.e. suspension to be filtered) is crucial for microfiltration optimization, its effect on membrane fouling has been relatively well documented, especially for fruit juices (Dahdouh et al., 2016). However, only a few studies on fruit juice microfiltration are referenced using a more local approach, characterizing the properties of the deposit layer on the membrane, or the behavior of concentrated suspended solids, as for instance has been done for other applications (e.g. alginate (Sioutopoulos et al., 2013)).

In this context, the objective of this work was to characterize the fouling propensity of orange juice matrices composed of concentrated suspended particles (CSP) with well-defined size distributions. The innovative methodology was first based on a fractionation of the orange juice by centrifugation to isolate and concentrate three specific size classes of suspended particles. These three specific size classes (i.e. small-, medium- and large-CSP) were then mixed together according to a mixture design (ABCD design) to generate various mixtures (CSP mixtures) with different particle size distributions. The fouling propensity of the CSP was evaluated at lab-scale through a permeability test, making it possible to measure the specific resistance to filtration and the compressibility factor, conventionally adopted to characterize the fouling propensity of a filtration deposit layer. In parallel, the rheological properties of these CSP were also evaluated in relation with their size distribution, using oscillatory measurements. The choice of studying the CSP viscoelastic behavior was motivated first by illustrating the CSP particle-particle interactions, and secondly by accessing data on the CSP behavior when subjected to shear stresses. This study aimed at providing new insights for a better optimization of microfiltration through the choice of relevant operating conditions (e.g. pretreatment, membrane configuration, hydrodynamic conditions) likely to limit the fouling propensity of suspended particles accumulated on the membrane surface.

2. Materials and methods

2.1. Orange juice selection and fractionation

The test matrix used for this study was a commercial orange juice (Andros “Squeezed oranges, 100% pure juice”, Andros, France) with the following physico-chemical characteristics: pH of 3.7 ± 0.02, citric acid of 0.96 ± 0.09 g/100 g, dry matter of 11.7 ± 0.02 g/100 g, °Bx of 11.4 ± 0.0 and turbidity of 3083 ± 144 NTU. These characteristics were measured at 25 °C in triplicate, according to conventional protocols and methods used for fruit juices, and described by Dahdouh et al. (2015).

The fractionation of the orange juice aimed at isolating suspended particles according to three approximate theoretical cutoff diameters (0.1, 1 and 10 μm). The cutoff diameters of 0.1 μm and 1 μm were chosen because particles with these sizes (close to the average pore diameters of membranes commonly used in microfiltration) are more likely to induce cake fouling (Bai & Leow, 2002). The third cutoff diameter of 10 μm was chosen to isolate the large particles of orange juice, commonly named pulp.

The fractionation was done by centrifugation (Centrifuge Model 5810 R, Eppendorf, Hamburg, Germany and Centrifuge Model Avanti J-E, Beckman Coulter, Indianapolis, USA) at different centrifugal acceleration/centrifugation time couples, according to a theoretical calculation based on Stokes’ law. Specific methodologies of dilution or concentration were proposed with the objective of obtaining, for each fraction, a standardized suspended solids content of about 11%.

The conditions of separation, dilution or concentration of the three specific particle size classes are detailed below:

(i) *Isolation of large-sized particles (> 10 μm):* Aliquots of 40 mL of homogenized juice were centrifuged at 500×*g* for 2 min to isolate the large particles. The settled particles, were centrifuged again at 18000×*g* for 60 min to eliminate interstitial dispersing phase and increase their initial concentration around 3% to about 11%.
(ii) *Isolation of medium-sized particles (between 1 μm and 10 μm):* Aliquots of 200 mL of the previous supernatant (i) were centrifuged at 3000×*g* for 10 min. Since the concentration of suspended particles was around 11%, these medium-sized particles did not undergo any additional centrifugation.
(iii) *Isolation of small-sized particles (between 0.1 μm and 1 μm):* Aliquots of 200 mL of the previous supernatant (ii) were centrifuged at 35000×*g* for 140 min. The settled particles were diluted with the supernatant (iii) to reduce their initial concentration (around 21%) to about 11%.

These three specific size classes, named respectively small-, medium- and large-CSP, were then mixed together according to a mixture design (ABCD design) to generate CSP mixtures with different proportions of these specific size -classes.

2.2. Physicochemical characterization of CSP

2.2.1. Particle size distribution measurement

Particle size distribution was determined by laser diffraction using a Malvern Mastersizer (Mastersizer 3000, Malvern Instruments Limited, Worcestershire, UK). The measurements were carried out in a wet mode, using distilled water as the suspension medium. The values of 1.73 and 1.33 were used for the refractive indices of particles and dispersion phase (water), respectively, and 0.1 was used for the absorption index of the particles. Measurements were carried out in triplicate on each sample with an obscuration of 42% and under stirring at 1500 rpm. For each measurement, size distribution (volume density against particle size) was provided, and the commonly used average diameter D [3;2] (Sauter mean diameter) was estimated. This average diameter, which represents the diameter of a sphere that has the same volume/surface ratio as the set of particles, was quantified since it characterizes the specific surface area, particularly important in liquid-solid interactions.

The particle size distribution measurement was only measured on the small-, medium- and large-CSP and not on the CSP mixtures.

2.2.2. Rheological properties evaluation

All the rheological measurements were performed using a controlled-stress Rheometer (Model Physica MCR301, Anton Paar Gmbh, Graz, Austria) equipped with Start Rheoplus software to record the experimental data. All the measurements were conducted at 25 ± 0.1 °C using a Peltier system and a Viscotherm VT 2 fluid circulator. The rheometer was supplied with a chamber previously sprayed with water to prevent dehydration of the sample during the measurements. Before rheological measurements, CSP (i.e. small-, medium-, large-CSP and CSP mixtures) were subjected to a resting period of 30 min before spreading on the rheometer. This step reduced the impact of mechanical strains (applied to the mixtures during their preparation) on the measured rheological parameters of the deposit layer.

Oscillatory strain sweep tests including a resting time of 10 min followed by a strain variation from 0.01 to 500% at a constant frequency of 1 Hz were performed for all trials using serrated parallel plates (PP25, Ø = 25 mm), with a 2 mm gap. For small-CSP, serrated parallel plates with a 50 mm diameter and a 1 mm gap were exceptionally used to ensure that the sample was kept between the plates during measurements (sample flows easily). All experiments were repeated at least

Table 1
Mass proportions of small-, medium- and large-CSP used in the 13 different runs, according to the mixture design.

Runs	Small-CSP (%)	Medium-CSP (%)	Large-CSP (%)
1	33	33	33
2	0	0	100
3	0	100	0
4	17	17	67
5	50	50	0
6	100	0	0
7	33	33	33
8	17	67	17
9	50	0	50
10	0	50	50
11	0	0	100
12	67	17	17
13	33	33	33

twice to ensure the consistency of the results.

The evolution of the two shear moduli, shear elastic modulus G' (representing the material's stiffness and the energy recovered when the stress is released) and the shear loss modulus G" (representing the energy lost through friction, and molecular and particle motion) was recorded as a function of strain (%).

The linear viscoelastic region (LVE-R) of each sample was determined with an LVE-R limit defined by the strain causing a reduction in shear elastic modulus values of 5% (Kaboorani & Blanchet, 2014).

2.2.3. Specific resistance to filtration and compressibility factor evaluation

The specific resistance to filtration SRF and the compressibility factor n of small-, medium-, large-CSP and CSP mixtures were evaluated through a permeability test. A "pre-formed cake" approach based on measuring the water flow rate through a deposit layer was proposed (Li et al., 2006).

2 g of CSP was spread on a porous support (polyethersulfone membrane, with pore size 0.1 μm and filtration area 17 cm^2, Sartorius, Goettingen, Germany). The height of the deposit layer was standardized at 1 mm for 10 min, using a force and a distance sensor (TA-XT2, Stable micro Systems, London, UK) resulting in a compacting pressure varying between 10 and 30 kPa. The weight after standardization was checked using an electronic balance, and neither height nor mass changed significantly during the tests.

The compacted deposit layer and its support were then placed in an Amicon cell (model 8050, Millipore Corporation, USA). 25 mL of distilled water was introduced into the cell, and directed through the deposit layer at different pressures ΔP (200, 150 and 100 kPa), significantly higher than the compacting pressure. Cumulative volumes (V, m^3) of the filtered water were recorded over time (t, s). The water flow rate through the deposit layer, $\frac{dV}{dt}$, was time-independent for a defined pressure. All the tests were conducted at room temperature (25 ± 2 °C) in dead-end mode without stirring.

The specific resistance to filtration SRF ($m.kg^{-1}$) of the deposit layer was calculated according to (Eq. (1)), derived from Darcy's Law (Darcy, 1989), and assuming negligible resistance of the support compared to the deposit layer resistance:

$$SRF = \frac{\Delta P \times A^2}{\frac{dV}{dt} \times \mu \times W_c} \qquad \text{Eq.1}$$

where ΔP is the applied pressure (Pa), A is the filtration area (m^2), μ is the viscosity of the permeate (10^{-3} Pa.s), and W_c is the dry matter of the compacted CSP (kg).

The impact of the pressure on water flow through the deposit layer, and consequently on SRF, was investigated through calculating the compressibility factor n (Eq. (2)) (Tiller & Kwon, 1998):

$$SRF = SRF_0 \left(1 + \frac{\Delta P}{P_a}\right)^n \qquad \text{Eq.2}$$

where SRF_0 is a reference specific resistance to filtration ($m.kg^{-1}$), and P_a is a reference pressure (Pa).

The reference pressure P_a, assumed to be very low compared to ΔP (Heij, 1994), was considered as negligible. Eq. (2) was simplified in Eq. (3) and the compressibility factor n was evaluated by plotting, in logarithmic coordinates, SRF as a function of the working pressure.

$$SRF \approx \frac{SRF_0}{P_a{}^n}(\Delta P)^n \qquad \text{Eq.3}$$

2.3. Mixture design

A mixture design (ABCD) without constrain (13 runs, Table 1) made it possible to investigate the effect of the mass proportion of small-, medium- and large-CSP on the rheological properties, the specific resistance to filtration and the compressibility of the CSP mixtures. The mass proportion of small-, medium- and large-CSP varied between 0 and 100% (w/w) levels. Three experiments were repeated at 33% small-CSP, 33% medium-CSP and 33% large-CSP (central point of the studied domain) to estimate the pure error and lack of fit. The experiments were also repeated twice at 0% small-CSP, 0% medium-CSP and 100% large-CSP. The analyzed responses were (Y_1) the shear elastic modulus in the linear viscoelastic range (log(LVE-R G′), Pa), (Y_2) the specific resistance to filtration at 200 kPa (SRF_{200kPa}, $m.kg^{-1}$) and (Y_3) the compressibility factor (n, /). The shear elastic modulus in the linear viscoelastic region (LVE-R G') was expressed in logarithmic base with the objective of obtaining a normal distribution of this value and enabling the analysis.

Each response (Y) was modeled as a function of the three studied factors, to simultaneously evaluate the effect of small-, medium- and large-CSP proportions, and to estimate linear effects and interactions between these three specific size classes. A model was proposed and the model adequacies were checked by variance analyses (F test, $p < 0.05$ with a confidence level of 95%) and R^2 values. Data obtained were analyzed using response surface methodology by JMP software (JMP version 13.0.0 (SAS Institute, Inc., Cary, USA)).

2.4. Statistical analysis

All results were expressed as mean of several analyses with standard deviation < 10% in all cases. Multivariate analysis (Pearson's matrix) was applied to detect linear correlations between product attributes at the 0.05 significance level. The statistical analyses were performed using XLSTAT (XLSTAT version 2020.1.1 (Addinsoft, Paris, France)).

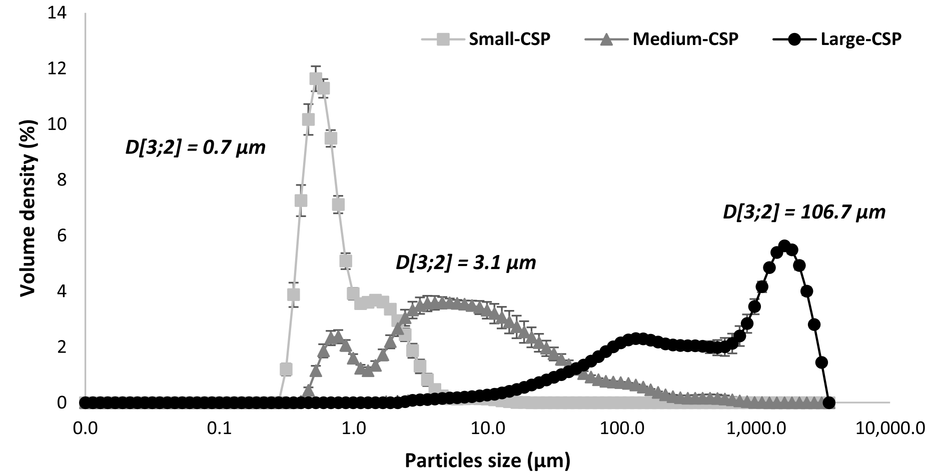

Fig. 1. Particle size distribution of small-, medium- and large-CSP, and their related surface area average diameters (D[3;2], μm).

3. Results and discussion

This section presents firstly the characteristics in terms of particle size distributions, viscoelastic behavior and fouling propensity of the three specific CSP of the orange juice (i.e. small-, medium- and large-CSP). Secondly, the characteristics of the CSP mixtures were presented and analyzed through the mixture design, established from the 13 experimental runs.

3.1. Characterization of small-, medium- and large-CSP

3.1.1. Particle size distribution

The particle size distributions and the Sauter diameter D [3;2] of the small-, medium- and large-CSP are presented in Fig. 1.

The particle size distributions of these three specific CSP were considered as bimodal and polydisperse. It can be observed that the small-CSP consisted mainly of particles smaller than 4 μm, with two modes around 0.5 and 1.5 μm. The medium-CSP were characterized by a wide range of size, between 0.5 and 250 μm, with two modes around 0.7 and 4.6 μm. Particles larger than 10 μm, with two modes around 145 μm and 1900 μm, characterized the large-CSP.

As a result of the above observations, the Sauter mean diameter, D [3;2], was significantly different for small-, medium- and large-CSP. Indeed, the large-CSP were distinguished by the highest value of D [3;2] (i.e. 106.7 μm). D[3;2] of medium- and small-CSP were respectively equal to 3.1 μm and 0.7 μm.

It should be observed that even if it was not possible to achieve exactly the targeted cut-off diameters theoretically imposed by the centrifugation (2.1), the adopted fractionation strategy did make it possible to isolate successfully the three following distinct particles size classes: (i) the large particles size class mainly consisted of pulp i.e. cell clusters due to undissociated parenchyma cells or individual cells (Espinosa-Muñoz et al., 2013), (ii) the medium particles size class mainly constituted of supra-colloids (individual cells, cell wall residues consisting of polyosides such as pectins, cellulose, hemicellulose and proteins) and (iii) the small particles size class consisting of colloids (proteins and polyosides such as pectin) (Dahdouh et al., 2016; Dahdouh et al., 2018).

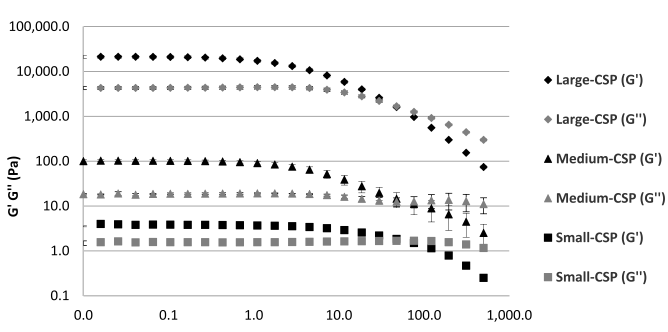

Fig. 2. Evolution of the shear elastic (G′) and the shear loss (G″) moduli (Pa) as a function of the strain (%) for small-, medium- and large-CSP.

3.1.2. Viscoelastic behavior

The two shear moduli, shear elastic G′ and the shear loss G″ moduli were plotted against the strain (%), on the logarithmic coordinates for small-, medium- and large-CSP (Fig. 2).

The same viscoelastic behavior was observed for the three specific CSP: a first period (below a strain of 5%), characterizing the linear viscoelastic region (LVE-R), where both shear elastic G′ and loss G″ moduli remained steady, and a second period where the moduli decreased as strain increased.

In the linear viscoelastic region, the shear elastic modulus was higher than the loss modulus, showing a predominance of a solid-like behavior (G’ > G″). Above a strain of 5%, G′ and G″ values decreased until reaching a critical strain where G″ became greater than G′, indicating a transition from a solid-like behavior to a viscous-like behavior (G’ < G”) for the three specific CSP. The tendency observed here, in which solid-like behavior was predominant in the linear domain, has been reported by many authors studying fruit-based suspensions (Dahdouh et al., 2016; Ricci et al., 2020; Leverrier et al., 2016; Labaky et al., 2021).

Though a solid-like behavior was found for all three specific CSP, their respective values of shear elastic and loss moduli were significantly different. The analysis of LVE-R G′ and LVE-R G″ underlines that large-CSP had the higher moduli with a LVE-R G’ (around 20000 Pa) 200 times greater than the LVE-R G′ of medium-CSP (around 100 Pa), which was in turn 25 times higher than value of the LVE-R G’ of small-CSP (around 4 Pa). Consequently, it emerges that small suspended particles had the lowest shear moduli, which is consistent with the literature (Labaky et al., 2020). As a result, orange juice pulp seems to constitute a network with higher interactions compared to the colloids or supra-colloids.

It should be mentioned that the LVE-R G’ values obtained for the three specific CSP were consistent with the ones obtained by (Ricci et al., 2020) for concentrated orange juices, ranging from 10 to 10 000 Pa (suspended solids content ranging from 2.1 to 11.0%).

3.1.3. Specific resistance to filtration and compressibility factor

Fig. 3 presents, for 100, 150 and 200 kPa, the specific resistance to filtration SRF and the compressibility factor n of small-, medium- and

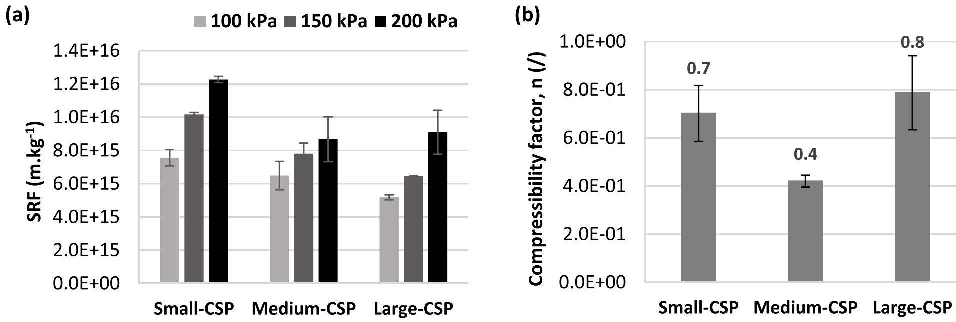

Fig. 3. Specific resistance to filtration SRF (m.kg[-1]) (a) and compressibility factor n (/) (b) for small-, medium- and large-CSP.

large-CSP.

The results showed that, regardless of the pressure applied, SRF was in the same range for large- and medium-CSP, whereas it was higher in the case of small-CSP (Fig. 3, (a)). (Bourcier et al., 2016) reported similar trends for mineral particles where the smaller the particles were in size, the higher their specific resistance to filtration was. These observations were in line with the well-known Kozeny-Carman equation, which shows that an increase in the particle specific surface area, and consequently a decrease in the Sauter diameter, results in an increase in the specific resistance to filtration (Carman, 1997).

Considering the influence of the applied pressure value, results show that SRF seems to increase with increasing pressure, suggesting a compressibility behavior for small-, medium- and large-CSP (Fig. 3, (a)).

Plotting SRF in logarithmic coordinates as a function of the filtration pressure (data not shown) made it possible to calculate the compressibility factor n. For the three specific CSP, the n values ranged between 0.4 and 0.8 (/) confirming that the greater the pressure applied, the greater the specific resistance (n significantly above 0). However, all three specific CSP could be considered as moderately compressible (Tiller & Kwon, 1998). It can be observed that small- and large-CSP had similar compressibility factors (around 0.7 and 0.8), whereas medium-CSP was characterized by a lower compressibility factor of 0.4 (/).

In conclusion, a deposit layer of orange juice colloids seems to have a higher fouling propensity than a deposit layer of supra-colloids or large particles, while a deposit layer of supra-colloids seems to present a lower compressibility.

3.2. Viscoelastic behavior, specific resistance to filtration and compressibility factor of CSP mixtures

3.2.1. Mixture design analyses

The shear elastic modulus was used for the study of the CSP mixtures'

Table 2
Predictive model equations for (Y_1) the normalized shear elastic modulus in the linear viscoelastic range (log(LVE-R G'), Pa), (Y_2) the specific resistance to filtration at 200 kPa (SRF_{200kPa}, $m.kg^{-1}$) and (Y_3) the compressibility factor n (/) indicating effect of each CSP-mixture component (X_1: large-CSP; X_2: medium-CSP and X_3: small-CSP) and their interactions.

Responses	Predictive model equations	R^2	P value
Log (LVE-R G')	$Y_1 = 4.27X_1 + 2.02X_2 + 0.66X_3 + 1.76\ X_1X_2 + 4.20X_1X_3 - 0.94X_2X_3 + 9.76X_1X_2\ X_3$	0.98	<0.0001[a]
SRF_{200kPa}	$Y_2 = 9.99.10^{15}X_1 + 6.96.10^{15}X_2 + 1.12.10^{16}X_3 + 1.58.\ 10^{16}X_1X_2 + 2.34.10^{16}X_1X_3 + 2.36.10^{16}X_2X_3 + 2.88.10^{17}X_1X_2\ X_3$	0.80	0.0004[a]
n	$Y_3 = 0.76X_1 + 0.37X_2 + 0.66X_3 - 1.02\ X_1X_2 - 0.89\ X_1X_3 + 0.98X_2X_3 + 7.67X_1X_2\ X_3$	0.70	0.0002[a]

[a] α = 0.05, Variance analyses (Fisher test).

Table 3
Summary of linear effects and interactions for (Y_1) the normalized shear elastic modulus in the linear viscoelastic range (log(LVE-R G'), Pa) (Y_2) the specific resistance to filtration at 200 kPa (SRF_{200kPa}, $m.kg^{-1}$) and (Y_3) the compressibility factor n (/).

Effects	P value Log(LVE-R G')	P value SRF_{200kPa}	P value n
Large-CSP	<0.00001[a]	0.02608[a]	0.00034[a]
Medium-CSP	0.00007[a]	0.19201	0.04228[a]
Small-CSP	0.01916[a]	0.05657[a]	0.00391[a]
Large-CSP*Medium-CSP	0.12490	0.51117	0.19300
Large-CSP*Small-CSP	0.000536[a]	0.34133	0.25125
Medium-CSP*Small-CSP	0.39892	0.36069	0.22763
Large-CSP*Medium-CSP*Small-CSP	0.13868	0.07043[a]	0.10629[a]

[a] α = 0.1.

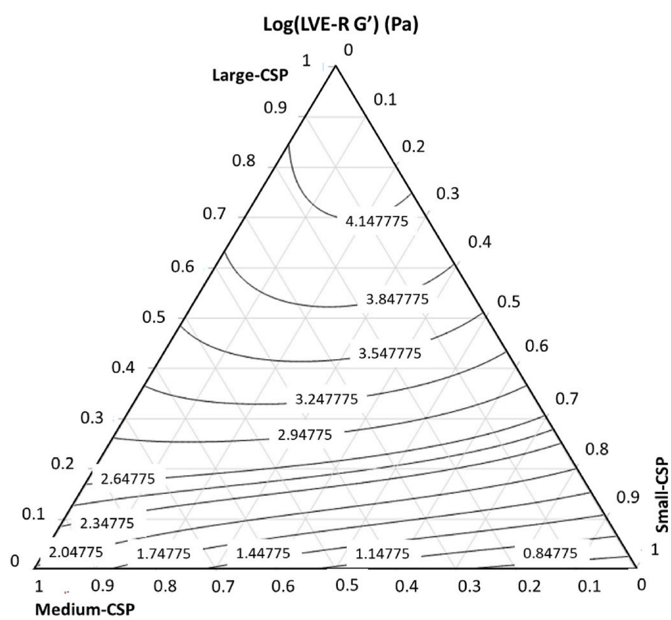

Fig. 4. Ternary diagram and response isosurfaces for (Y1) the normalized shear elastic modulus in the linear viscoelastic range (log(LVE-R G'), Pa).

rheological behavior (solid-like behavior). The specific resistance to filtration at 200 kPa was chosen for the analysis of the CSP mixtures because the results were more consistent than those obtained at 150 and 100 kPa.

Tables 2 and 3 give information about the statistically validated models. The predictive models presented in Table 2 were used to

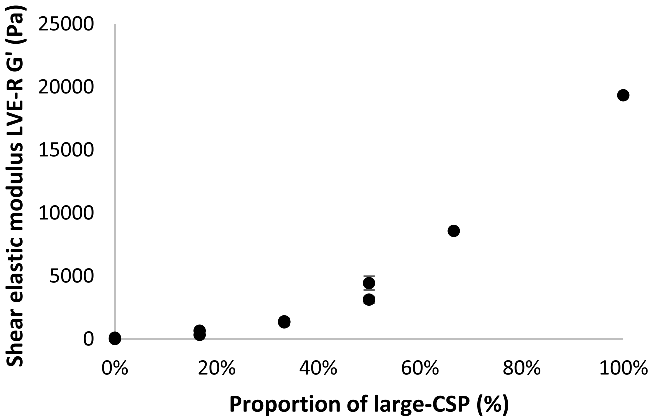

Fig. 5. Evolution of the shear elastic modulus (LVE-R G′, Pa) as a function of the proportion of large-CSP (%).

establish ternary diagrams and response isosurfaces. These illustrations are relevant to investigate the role of the three specific size classes on the CSP mixtures' viscoelastic behavior, specific resistance to filtration and compressibility factor.

3.2.2. Viscoelastic behavior of CSP mixtures

Fig. 4 presents ternary diagrams and response isosurfaces related to the influence of the mass proportion of small-, medium- and large-CSP on the LVE-R G' of CSP mixtures.

Though a solid-like behavior was found for all the CSP mixtures (the 13 experimental runs, data not shown), these mixtures presented significantly different shear elastic modulus values, as illustrated in Fig. 4. The log(LVE-R G′) values increased with the increase in the proportion of large-CSP (same trend observed for the shear loss modulus, data not shown). The respective proportion of medium- and small-CSP in the mixtures did not seem to have an impact on the log (LVE-R G′) values, which therefore appeared to be only dependent on the presence of the large-CSP. This observation was clearly underlined by the graphic representation of the shear elastic modulus (LVE-R G') as a function of the proportion of large-CSP (%), in any proportion of small- and medium-CSP (Fig. 5).

Based on these results, it could be also suggested that the biochemical nature of large-CSP (i.e. pulp, cell clusters or fragments) might enhance particles interactions, which is not the case for small- and medium-CSP (i.e. proteins, colloidal polyosides, cell wall residues, individual cells). The behavior of the CSP mixtures and the role of the large-CSP were consistent with literature showing that the proportion of large particles enhanced the LVE-R G' of fruit purees (Espinoza-Munoz, 2013; Labaky et al., 2020). However, this observation should be nuanced since some other studies do not emphasize the same statement (Azeem et al., 2020). This difference could be attributed to different distribution of the biochemical compounds in each size-class from one study to another. Some authors explain that experimental protocols for obtaining the size fractions (i.e. centrifugation, grinding), but also the fruit variety or maturation state, could influence the biochemical nature of the compounds present in each size class (Schijvens et al., 1998).

3.2.3. Specific resistance to filtration and compressibility factor of CSP mixtures

Fig. 6 presents ternary diagrams and response isosurfaces related to the influence of the different size class proportions in the CSP mixtures on the specific resistance to filtration SRF_{200kPa} (Fig. 6, (a)) and n (Figure (6), (b)).

When considering ternary diagrams and response isosurfaces in relation with SRF_{200kPa}, it emerges that the simultaneous presence of small-, medium- and large-CSP resulted in higher specific resistances to filtration (Fig. 6 (a)). Thus, SRF_{200kPa} reached the value of $2.6.10^{16}$ m. kg^{-1} for the mixture containing simultaneously and equally the three specific CSP (central point), whereas the specific resistances to filtration of the three specific CSP did not exceed $1.2.10^{16}$ m.kg^{-1} (Fig. 3 (a)). While the simultaneous presence of the three size classes led to the highest fouling propensity, Fig. 6 (a) demonstrated that SRF_{200kPa} decreased when one of the three size classes, whichever it was, decreased in proportion. Consequently, it seemed that greater the size polydispersity was, greater the fouling propensity was. Similar results were obtained for SRF_{100kPa} and SRF_{150kPa} (ternary diagrams not shown).

The key role of the size polydispersity on the specific resistance to filtration was consistent with stacking models of granular particles. Indeed, these models demonstrate that the porosity of a medium decreases when two particle size classes are mixed together, and continues to decrease when the particle polydispersity increases (Averardi et al., 2020; Roquier, 2015). This decrease in porosity is explained by spaces

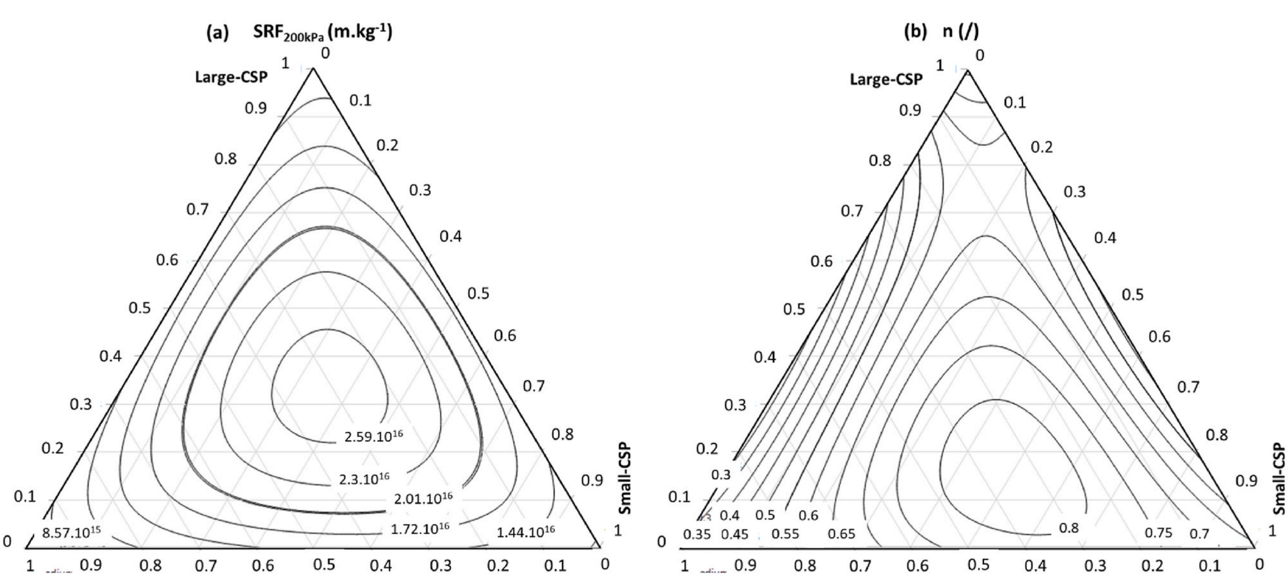

Fig. 6. Ternary diagrams and response isosurfaces for (Y_2) the specific resistance to filtration at 200 kPa (SRF_{200kPa}, m.kg^{-1}) (a) and (Y_3) the compressibility factor (n, /) (b).

between large particles that are occupied by smaller particles and so on. A deposit layer consisting of various size particles represents thus a low-porosity medium with a high tortuosity, resulting in a high specific resistance to filtration (Bourcier et al., 2016).

Fig. 6 (b) illustrates the influence of small-, medium- and large-CSP on the compressibility factor of the CSP mixtures. It was first observed that the lowest n values (<0.6) were obtained when the proportion of small-CSP was less than 15%. In these conditions, the increase of the medium-CSP proportion led to lower n values. Conversely, the highest n (higher to 0.6) were obtained as soon as the small-CSP proportion exceeded 20%. These observations could be attributed respectively to the low intrinsic compressibility of the medium-CSP and the high intrinsic compressibility of the small-CSP (Fig. 3 (b)). Thus, while an increase of the medium-CSP proportion tended to decrease the compressibility factor, an increase in the small-CSP proportion tended to increase it. Even if the large-CSP presented an intrinsically high n value (Fig. 3 (b)), their role on the compressibility factor was negligible when mixed with other size classes. Indeed, large-CSP proportion never seemed to influence the n values, which thus appeared to depend essentially on the small- and medium-CSP.

Some authors underlined the role of the smallest particles on the compressibility of a polydispersed-particles deposit. Indeed (Bourcier et al., 2016) reported that, with the application of a pressure, the smallest particles could move, leading to a rearrangement of all the different particle size classes, potentially leading to higher compressibility. However, it could be suggested that even if the particle size can have a role in the compressibility of the deposit layer, other factors may also influence this behavior, such as the shape of the particles (Bourcier et al., 2016) and their intrinsic deformability.

The response surfaces of the ternary diagrams demonstrated that a deposit layer with a low specific resistance to filtration could be obtained with the presence of only large- or medium-CSP, i.e. isolated cells and cell wall residues, known as stiff plant tissues (Kozioł et al., 2017). A layer deposit with low compressibility factor could be obtained by mixing large particles and supra-colloids, but with a very low proportion of colloids, or with only supra-colloids. According to these results and for fruit-based suspensions, it would therefore seem essential to favor the presence of medium-sized populations (i.e. supra-colloids) to limit the fouling properties of the deposit layer during microfiltration operation.

4. Conclusion

This work aimed at characterizing the viscoelastic behavior and the fouling propensity of orange juice matrices composed of concentrated suspended-particles (CSP) with well-defined size-distributions.

Small-, medium- and large-CSP (respectively colloids, supra-colloids and pulp or cell clusters) were characterized by viscoelastic properties with predominantly solid-like behavior. The shear elastic modulus was enhanced when increasing the proportion of large-CSP. The specific resistances to filtration were similar for large- and medium-CSP, but slightly higher in the case of small-CSP. Furthermore, small-, medium- and large-CSP deposit layers were associated with non-zero compressibility factor, attesting to increased specific resistance to filtration with pressure. It was also revealed that large- and small-CSP particles were more compressible than medium ones. The rheological behavior and the fouling propensity of mixtures of small-, medium- and large-CSP were analyzed using ternary diagrams. These diagrams revealed that the proportion of small-, medium- and large-CSP impacted in a different way the fouling propensity and the shear elastic modulus of CSP mixtures: the solid-like behavior was strongly influenced by large-CSP proportions, the specific resistance to filtration depended mainly on the size polydispersity of the CSP, while small- or medium-CSP proportions had a major influence on the compressibility factor.

Even if further research could highlight a direct link between these investigations and the choice of suitable microfiltration operating conditions, the innovative experimental strategies proposed in this study has provided new knowledge on the role of the size distribution of concentrated suspended particles on their rheological behavior and their fouling propensity.

CRediT authorship contribution statement

Camille Demoulin: Methodology, Software, Validation, Investigation, Writing – original draft, Visualization. **Christelle Wisniewski:** Conceptualization, Methodology, Validation, Formal analysis, Resources, Writing – review & editing, Visualization, Supervision. **Julien Ricci:** Conceptualization, Methodology, Software, Validation, Formal analysis, Investigation. **Michèle Delalonde:** Conceptualization, Methodology, Validation, Formal analysis, Resources, Writing – review & editing, Visualization, Supervision. **Layal Dahdouh:** Conceptualization, Methodology, Validation, Formal analysis, Resources, Writing – review & editing, Visualization, Supervision.

References

Averardi, A., Cola, C., Zeltmann, S. E., & Gupta, N. (2020). Effect of particle size distribution on the packing of powder beds: A critical discussion relevant to additive manufacturing. *Materials Today Communications, 24*, 100964. https://doi.org/10.1016/j.mtcomm.2020.100964

Azeem, M., Mu, T.-H., & Zhang, M. (2020). Influence of particle size distribution of orange-fleshed sweet potato flour on dough rheology and simulated gastrointestinal digestion of sweet potato-wheat bread. *Lebensmittel-Wissenschaft & Technologie, 131*, 109690. https://doi.org/10.1016/j.lwt.2020.109690

Bai, R., & Leow, H. F. (2002). Microfiltration of activated sludge wastewater—the effect of system operation parameters. *Separation and Purification Technology, 29*(2), 189–198. https://doi.org/10.1016/S1383-5866(02)00075-8

Bhattacharjee, C., Saxena, V. K., & Dutta, S. (2017). Fruit juice processing using membrane technology: A review. *Innovative Food Science & Emerging Technologies, 43*, 136–153. https://doi.org/10.1016/j.ifset.2017.08.002

Bourcier, D., Féraud, J. P., Colson, D., Mandrick, K., Ode, D., Brackx, E., & Puel, F. (2016). Influence of particle size and shape properties on cake resistance and compressibility during pressure filtration. *Chemical Engineering Science, 144*, 176–187. https://doi.org/10.1016/j.ces.2016.01.023

Carman, P. C. (1997). Fluid flow through granular beds. *Chemical Engineering Research and Design, 75*, S32–S48. https://doi.org/10.1016/S0263-8762(97)80003-2

Dahdouh, L., Delalonde, M., Ricci, J., Ruiz, E., & Wisnewski, C. (2018). Influence of high shear rate on particles size, rheological behavior and fouling propensity of fruit juices during crossflow microfiltration: Case of orange juice. *Innovative Food Science & Emerging Technologies, 48*, 304–312. https://doi.org/10.1016/j.ifset.2018.07.006

Dahdouh, L., Delalonde, M., Ricci, J., Servent, A., Dornier, M., & Wisniewski, C. (2016a). Size-cartography of orange juices foulant particles: Contribution to a better control of fouling during microfiltration. *Journal of Membrane Science, 509*, 164–172. https://doi.org/10.1016/j.memsci.2016.01.052

Dahdouh, L., Wisniewski, C., Ricci, J., Vachoud, L., Dornier, M., & Delalonde, M. (2016b). Rheological study of orange juices for a better knowledge of their suspended solids interactions at low and high concentration. *Journal of Food Engineering, 174*, 15–20. https://doi.org/10.1016/j.jfoodeng.2015.11.008

Dahdouh, L., Wisniewski, C., Kapitan-Gnimdu, A., Servent, A., Dornier, M., & Delalonde, M. (2015). Identification of relevant physicochemical characteristics for predicting fruit juices filterability. *Separation and Purification Technology, 141*, 59–67. https://doi.org/10.1016/j.seppur.2014.11.030

Darcy, H. (1989). "Determination of the Laws of Flow of Water Through Sand", Appendix to Histoire des Fontaines Publiques de Dijon, p590-595, 1856. *Republished on Fluid/Particle Separation Journal, 2*, 33–35.

Davis, R. H. (1992). Modeling of fouling of crossflow microfiltration membranes. *Separation and Purification Methods, 21*(2), 75–126. https://doi.org/10.1080/03602549208021420

Espinosa-Muñoz, L., Renard, C. M. G. C., Symoneaux, R., Biau, N., & Cuvelier, G. (2013). Structural parameters that determine the rheological properties of apple puree. *Journal of Food Engineering, 119*(3), 619–626. https://doi.org/10.1016/j.jfoodeng.2013.06.014

Heij, E. J., & L. (1994). *An analysis of sludge filtration and expression.* https://doi.org/10.6100/IR423039

Kaboorani, A., & Blanchet, P. (2014). Determining the linear viscoelastic region of sugar maple wood by dynamic mechanical analysis. *BioResources, 9*. https://doi.org/10.15376/biores.9.3.4392-4409

Kazemi, M. A., Soltanieh, M., & Yazdanshenas, M. (2012). Modeling of transient permeate flux decline during crossflow microfiltration of non-alcoholic beer with consideration of particle size distribution. *Journal of Membrane Science, 411*(412), 13–21. https://doi.org/10.1016/j.memsci.2012.02.064

Kozioł, A., Cybulska, J., Pieczywek, P. M., & Zdunek, A. (2017). Changes of pectin nanostructure and cell wall stiffness induced in vitro by pectinase. *Carbohydrate Polymers, 161*, 197–207. https://doi.org/10.1016/j.carbpol.2017.01.014

Kromkamp, J., Faber, F., Schroen, K., & Boom, R. (2006). Effects of particle size segregation on crossflow microfiltration performance: Control mechanism for concentration polarisation and particle fractionation. *Journal of Membrane Science, 268*(2), 189–197. https://doi.org/10.1016/j.memsci.2005.06.012

Labaky, P., Dahdouh, L., Ricci, J., Wisniewski, C., Pallet, D., Louka, N., & Grosmaire, L. (2021). Impact of ripening on the physical properties of mango purees and application of simultaneous rheometry and in situ FTIR spectroscopy for rapid identification of biochemical and rheological changes. *Journal of Food Engineering, 300*, 110507. https://doi.org/10.1016/j.jfoodeng.2021.110507

Labaky, P., Grosmaire, L., Ricci, J., Wisniewski, C., Louka, N., & Dahdouh, L. (2020). Innovative non-destructive sorting technique for juicy stone fruits: Textural properties of fresh mangos and purees. *Food and Bioproducts Processing, 123*, 188–198. https://doi.org/10.1016/j.fbp.2020.06.013

Laorko, A., Tongchitpakdee, S., & Youravong, W. (2013). Storage quality of pineapple juice non-thermally pasteurized and clarified by microfiltration. *Journal of Food Engineering, 116*(2), 554–561. https://doi.org/10.1016/j.jfoodeng.2012.12.033

Leverrier, C., Almeida, G., Espinosa-Mu noz, L., & Cuvelier, G. (2016). Influence of particle size and concentration on rheological behaviour of reconstituted apple purees. *Food Biophysics, 11*(3), 235–247. https://doi.org/10.1007/s11483-016-9434-7

Li, W., Kiser, C., & Richard, Q. (2006). *Development of A Filter cake permeability test methodology* (Vol. 6).

Miyoshi, T., Yuasa, K., Ishigami, T., Rajabzadeh, S., Kamio, E., Ohmukai, Y., Saeki, D., Ni, J., & Matsuyama, H. (2015). Effect of membrane polymeric materials on relationship between surface pore size and membrane fouling in membrane bioreactors. *Applied Surface Science, 330*, 351–357. https://doi.org/10.1016/j.apsusc.2015.01.018

de Oliveira, R. C., Docê, R. C., & de Barros, S. T. D. (2012). Clarification of passion fruit juice by microfiltration: Analyses of operating parameters, study of membrane fouling and juice quality. *Journal of Food Engineering, 111*(2), 432–439. https://doi.org/10.1016/j.jfoodeng.2012.01.021

Razi, B., Aroujalian, A., & Fathizadeh, M. (2012). Modeling of fouling layer deposition in cross-flow microfiltration during tomato juice clarification. *Food and Bioproducts Processing, 90*(4), 841–848. https://doi.org/10.1016/j.fbp.2012.05.004

Ricci, J., Delalonde, M., Wisnewski, C., & Dahdouh, L. (2020). Role of dispersing and dispersed phases in the viscoelastic properties and the flow behavior of fruit juices during concentration operation: Case of orange juice. *Food and bioproducts processing*. https://doi.org/10.1016/j.fbp.2020.11.013

Roquier, G. (2015). *Le modèle d'Empilement compressible 4-paramètres*. Rencontres Universitaires de Génie Civil. https://hal.archives-ouvertes.fr/hal-01167749.

Rouquié, C., Dahdouh, L., Ricci, J., Wisniewski, C., & Delalonde, M. (2019). Immersed membranes configuration for the microfiltration of fruit-based suspensions. *Separation and Purification Technology, 216*, 25–33. https://doi.org/10.1016/j.seppur.2019.01.062

Schijvens, E. P. H. M., Vliet, T. van, & Dijk, C. van (1998). Effect of processing conditions on the composition and rheological properties of applesauce. *Journal of Texture Studies, 29*(2), 123–143. https://doi.org/10.1111/j.1745-4603.1998.tb00160.x

Sioutopoulos, D. C., Goudoulas, T.B., Kastrinakis, E. G., Nychas, S. G., & Karabelas, A. J. (2013). Rheological and permeability characteristics of alginate fouling layers developing on reverse osmosis membranes during desalination. *Journal of Membrane Science, 434*, 74–84. https://doi.org/10.1016/j.memsci.2013.01.018

Tiller, F. M., & Kwon, J. H. (1998). Role of porosity in filtration: XIII. Behavior of highly compactible cakes. *AIChE Journal, 44*(10), 2159–2167. https://doi.org/10.1002/aic.690441005

Ushikubo, F. Y., Watanabe, A. P., & Viotto, L. A. (2007). Microfiltration of umbu (Spondias tuberosa Arr. Cam.) juice. *Journal of Membrane Science, 288*(1), 61–66. https://doi.org/10.1016/j.memsci.2006.11.003

Vaillant, F., Cisse, M., Chaverri, M., Perez, A., Dornier, M., Viquez, F., & Dhuique-Mayer, C. (2005). Clarification and concentration of melon juice using membrane processes. *Innovative Food Science & Emerging Technologies, 6*(2), 213–220. https://doi.org/10.1016/j.ifset.2004.11.004

Vaillant, F., Millan, P., O'Brien, G., Dornier, M., Decloux, M., & Reynes, M. (1999). Crossflow microfiltration of passion fruit juice after partial enzymatic liquefaction. *Journal of Food Engineering, 42*(4), 215–224. https://doi.org/10.1016/S0260-8774(99)00124-7

Yu, J., & Lencki, R. W. (2004). Effect of enzyme treatments on the fouling behavior of apple juice during microfiltration. *Journal of Food Engineering, 63*(4), 413–423. https://doi.org/10.1016/j.jfoodeng.2003.08.013